D D C

RECEIVED

AUG 2 1976

A

A Synopsis of Studies on the Interaction of Low Frequency Acoustic Signals With the Ocean Bottom

Salvatore R. Santaniello
Frederick R. DiNapoli
Robert K. Dullea
Peter D. Herstein
Ocean Sciences and Technology Department

30 June 1976

NUSC

NAVAL UNDERWATER SYSTEMS CENTER
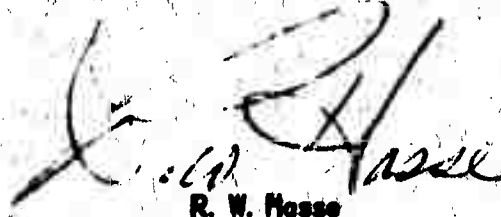Newport,Rhode Island • New London,Connecticut

UNCLASSIFIED

NUSC-TD-5337

REPORT DOCUMENTATION PAGE		READ INSTRUCTIONS BEFORE COMPLETING FORM
1. REPORT NUMBER TD 5337	2. GOVT ACCESSION NO.	3. RECIPIENT'S CATALOG NUMBER
4. TITLE (and Subtitle) A SYNOPSIS OF STUDIES ON THE INTERACTION OF LOW FREQUENCY ACOUSTIC SIGNALS WITH THE OCEAN BOTTOM.		5. TYPE OF REPORT & PERIOD COVERED Technical document 6. PERFORMING ORG. REPORT NUMBER
7. AUTHOR(s) Salvatore R. Santaniello Robert K. Dullea Frederick R. DiNapoli Peter D. Herstein		8. CONTRACT OR GRANT NUMBER(s)
9. PERFORMING ORGANIZATION NAME AND ADDRESS Naval Underwater Systems Center New London Laboratory New London, Connecticut 06320		10. PROGRAM ELEMENT, PROJECT, TASK AREA & WORK UNIT NUMBERS
11. CONTROLLING OFFICE NAME AND ADDRESS Naval Sea Systems Command (SEA 06H1-4) Washington, D. C. 20362		12. REPORT DATE 30 June 1976 13. NUMBER OF PAGES 42
14. MONITORING AGENCY NAME & ADDRESS(If different from Controlling Office)		15. SECURITY CLASS. (of this report) UNCLASSIFIED 15a. DECLASSIFICATION/DOWNGRADING SCHEDULE

16. DISTRIBUTION STATEMENT (of this Report)

Approved for public release; distribution unlimited.

NUSC-A-650-06
SF52-552

17. DISTRIBUTION STATEMENT (of the abstract entered in Block 20, if different from Report)

SF52-552-602, SF52-552-601

18. SUPPLEMENTARY NOTES

19. KEY WORDS (Continue on reverse side if necessary and identify by block number)

Bottom Loss Measurements
Propagation Loss Modeling
Ocean Bottom Modeling
Deconvolution Processing

Ocean Sediment Impulse Responses
Ocean Sediment Sound Refraction

20. ABSTRACT (Continue on reverse side if necessary and identify by block number)

Understanding the mechanisms by which the ocean sediment redirects impinging sound back into the ocean is necessary in developing propagation models for SONAR performance prediction. Thus, NUSC has (1) conducted controlled, self-calibrating acoustic measurements where the bottom interacted signal is isolated in time for analysis, (2) developed deconvolution processing techniques to aid in describing the impulse response of the ocean sediment and (3) performed modeling to study the
(over)

DD FORM 1473 EDITION OF 1 NOV 65 IS OBSOLETE
1 JAN 73
S/N 0102-014-6601

UNCLASSIFIED

20. ABSTRACT (Cont'd)

interaction of acoustic waves at the ocean bottom. This document presents a synopsis of the studies primarily showing the necessity to consider the refraction of sound by the ocean sediment when predicting low frequency propagation loss. Sediment refraction of sound and reflection of sound by the sediment interface and subbottom layering are the causes for the negative bottom loss phenomenon and for a given frequency bandwidth dependence and receiver depth dependence of bottom loss. Deconvolution analyses have aided in time resolution of intrapulse signals that make up the bottom interacting arrivals. Resolution of these arrivals aids in interpreting results. The FFP modeling effort provides quantitative evidence for the necessity to consider the refraction of sound by the ocean sediment to properly interpret low frequency propagation loss measurements in areas where the ocean bottom plays an important part.

TABLE OF CONTENTS

LIST OF ILLUSTRATIONS

FOREWORD

It is well known that the ocean bottom refracts, as well as reflects, acoustic energy. Along with other acousticians, we at the Naval Underwater Systems Center, New London Laboratory (NUSC/NLL) are interested in the extent to which the refraction and reflection phenomena influence the transmission of low frequency (<500 Hz) sound through the ocean. Furthermore, we are interested in the physical properties of the sediment which control these phenomena, and in how well we must know these properties to predict propagation characteristics. This technical document has been assembled from four companion papers presented at the 90th Meeting of the Acoustical Society of America, San Francisco, on 5 November 1975 to synopsize our present endeavors with regard to this interest.

A SYNOPSIS OF STUDIES ON THE INTERACTION
OF LOW FREQUENCY ACOUSTIC SIGNALS
WITH THE OCEAN BOTTOM

I. LOW FREQUENCY NEGATIVE BOTTOM LOSS--
AN EFFECT OF THE OCEAN BOTTOM'S ACTING
AS A FOCUSING MECHANISM*

INTRODUCTION

To acquire an understanding of the transmission of low frequency sound through the ocean, it is mandatory that propagation models account for the refraction of acoustic energy by the ocean bottom. The propagation model must be able to accommodate the complete environmental description of the water column and sediment. Studies conducted by the Naval Underwater Systems Center New London Laboratory (NUSC/NLL) have led to the viewpoint that developing such a model for predicting low frequency propagation loss is more meaningful than extending high frequency measurement and analysis techniques to obtain low frequency bottom loss values for use with less complete propagation models. This section is concerned with the origin of this viewpoint which evolved specifically through analysis of low frequency bottom loss data acquired by using a self-calibrating measurement technique. These data further stimulated the analyses and modeling studies that are discussed in the following three sections of this document.

DISCUSSION

Distinction Between Bottom Loss and Bottom-Reflection Loss

In general, acousticians describe an acoustic signal's interaction with the ocean bottom in terms of a single function: the reflection coefficient. A typical geoacoustic model that yields the plane-wave reflection coefficient as a function of angle and frequency considers an infinite single-frequency plane wave to be incident at only one angle with the ocean bottom. The bottom is assumed to have smooth-parallel boundaries where the layer thickness, density, sound speed, sound-speed gradient, and attenuation are input parameters. The coefficient may be defined as the ratio of reflected-to-incident acoustic intensities and the logarithm of the coefficient is called BOTTOM-REFLECTION LOSS.[1] To measure bottom-reflection loss within the constraints of this definition is virtually impossible. In practice, it is estimated through an indirect approach that requires interpretation.

*This section was authored by S. R. Santaniello.

The approach is first to measure the propagation loss of an acoustic pulse that traversed the medium from source to receiver along the acoustic path that has enabled the pulse to interact once with only the ocean bottom (PL_B). The second step is to calculate the water-column propagation loss for only the bottom-reflection path by assuming a flat, single-interface bottom that has a reflection coefficient of one (WPL_B). The final step is to compare the measured and calculated propagation losses; the difference is known as BOTTOM LOSS (BL),

$$BL = PL_B - WPL_B. \tag{1}$$

Thus bottom loss is a quantity that is extracted from a propagation loss measurement. The techniques under which this quantity is obtained, however, can result in the bottom loss being distinctively different from the actual bottom-reflection loss for some point (area) at the water-sediment interface of the ocean bottom region under study.

Relative Measurement of Bottom Loss

Because of water-region multipaths, considerable care and interpretation are required (especially for low grazing-angle data) to determine the propagation loss for the energy that has interacted only with the ocean bottom. At low frequencies, additional factors affect results, such as low frequency noise and knowing the exact source level for each detonation of an explosive.

When experiments are conducted in deep water, it is possible to minimize multipath and source level effects. By laterally separating an explosive source and a hydrophone, and positioning them well away from the ocean boundaries, the time separation between water-region arrivals can become sufficient to perform a relative bottom loss measurement to grazing angles below 5 degrees. With time-separated, pulsed-acoustic arrivals, the source level for the explosive can be determined by measuring the received level of the direct acoustic path arrival (RL_D) and calculating the water-column propagation loss for the direct arrival (WPL_D)

$$SL = RL_D + WPL_D. \tag{2}$$

With the measure of source level, the propagation loss for the time-separated bottom-interacting signal arrival can be determined by measuring the received level of that arrival (RL_B)

$$PL_B = SL - RL_B = RL_D + WPL_D - RL_B. \tag{3}$$

Substituting equation (3) into equation (1), the bottom loss calculation reduces to the differences between two ratios, shown in logarithmic form,

$$BL = (RL_D - RL_B) + (WPL_D - WPL_B). \tag{4}$$

The first ratio accounts for the difference between the energies of the direct and bottom-interacting arrivals, eliminating the necessity of knowing the source level for each detonation. The second ratio accounts for the difference between the calculated water-column propagation losses for the direct and bottom-reflection paths, and the direct path loss can be verified. Although source level, processing, and prediction errors are minimized, interpretation is still required, especially at low frequencies when subbottom refraction and reflection of acoustic energy occurs.

Interaction of Bottom-Reflected and Bottom-Refracted Signals

Consider an ideal Rayleigh plane-wave reflection curve for a two-layered, flat ocean bottom, as presented in figure 1A, which portrays a critical angle caused when the sediment sound-speed is greater than that of the water column. Consider also an omnidirectional impulsive point source and an acoustic path where energy impinges the sediment at a relatively low grazing angle θ_1 (figure 1B). Based on the plane-wave reflection curve, all energy is reflected. Consider next an acoustic path associated with energy which impinges on the sediment at a higher grazing angle θ_2 (figure 1B). This energy penetrates and traverses through the sediment. If a positive sound-speed gradient exists in the sediment, the energy will be refracted and returned to the water at a distance down range. If the travel time of the refracted energy is equal to the travel time of the reflected energy at some point in the medium, the arrival interpreted as being only a bottom-reflected arrival will actually contain additional interfering energy.

Experimental Description and Measurement Results

To show that concurrent bottom refracted and reflected arrivals appear to be affecting low frequency bottom loss measurements, we will discuss results of one of the experiments conducted by NUSC/NLL.[2] These results are not unique. Similar results from another experiment are presented in section IV.

The experimental geometry for the particular bottom loss results that will be subsequently discussed is shown at the top of figure 2. The data were acquired by using explosive sources detonated at a depth of 900 meters, whereas the hydrophone was at 1700 meters in water 4100 meters deep. The hydrophone was contained in an instrumented self-recording submersible buoy known as AUTOBUOY.[3] Thus, low frequency noise was kept to a minimum. The geometry was optimized to ensure that the bottom-interacting energy could be isolated at low grazing angles. For the time-separated sequence of acoustic arrivals shown in figure 2, the single-point grazing angle of the bottom arrival is 11.4 degrees. Bottom loss was obtained under the constraints of the previously discussed relative measurement approach. Data were processed over a two-octave band centered at the explosive's spectral peak and the results are presented in figure 3.

3

As can be observed in the figure, 17 values between 9 and 15 degrees form a smooth transition into and out of a region which, for lack of a better expression, has become known as the negative bottom loss region. Although these results are dependent upon the particular experimental configuration, it should be realized that since a relative measurement approach was used, experimental error was insignificant; therefore, all values are real. Negative values were consistently calculated over a considerable angle coverage, because more energy was received for the signal identified as the bottom-reflected arrival than could be accounted for by the water-column propagation loss model, which assumes that only a single bottom-reflected signal is involved in the reflection process. It is hypothesized that during the actual measurements, energy penetrated the ocean bottom at relatively high grazing angles, was refracted back into the water column and arrived at the hydrophone coincident in time with the low grazing-angle reflected energy. This premise can be qualitatively supported, to some degree, by observing ray-tracing diagrams.

Ray-Tracing Results

During all our recent experiments, the Lamont-Doherty Geological Observatory conducted wide-angle seismic reflectivity measurements to provide estimates of the sediment's thickness, interval sound speed, and sound-speed gradient. Thus a sediment sound-speed profile could be combined with a sound-speed profile of the water column to produce ray-tracing diagrams, one of which is presented in figure 4. This ray diagram is of interest simply because it demonstrates a concept found in current texts: the focusing of acoustic energy by the ocean bottom. The formation of a caustic is evident, and it appears possible that concurrent refracted and reflected arrivals could occur over a considerable volume of the water.

However, this discussion implies only that the ocean bottom is, in effect, partially focusing acoustic energy by refracting and reflecting sound. More quantitative evidence is required to show that refracted and reflected signals constructively interact, resulting in more energy being contained in the bottom-interacting arrival than can be accounted for by using the previously described bottom loss extraction procedure. The remaining sections of this document provide this evidence by presenting modeling studies and demonstrating how deconvolution processing can aid in analysis by isolating refracted and reflected signals within the time of the bottom-interacting arrival.
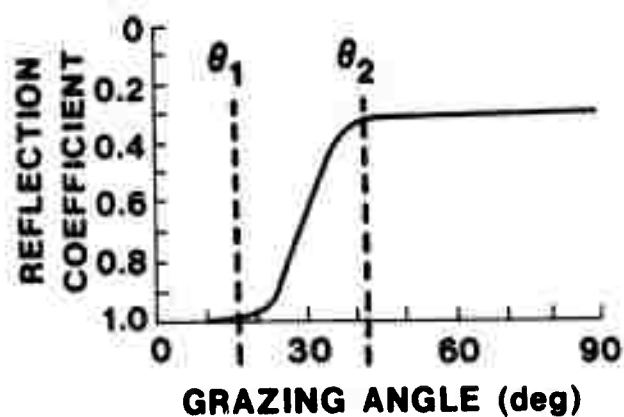
Figure 1A. Ideal Rayleigh Reflection Curve for Sediment
Sound Speed (c_B) Greater Than Water Sound Speed (c_W)
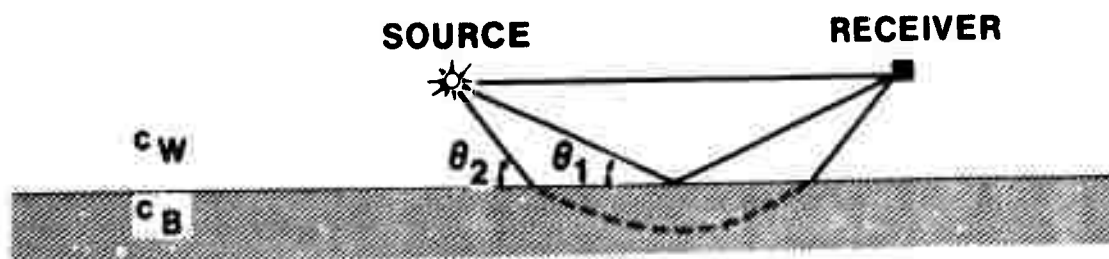
Figure 1B. Possible Mechanism Whereby Sediment Sound-Speed
Gradient Causes Sound to Refract and Interact With Sediment
Interface-Reflected Sound at a Point Down Range from Source

EXPERIMENTAL GEOMETRY
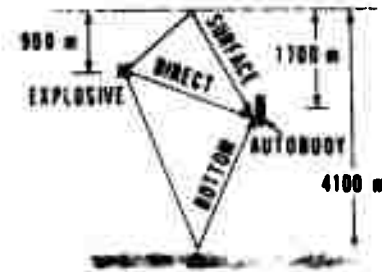
SEQUENCE OF ARRIVALS
GRAZING ANGLE = 11.4 deg
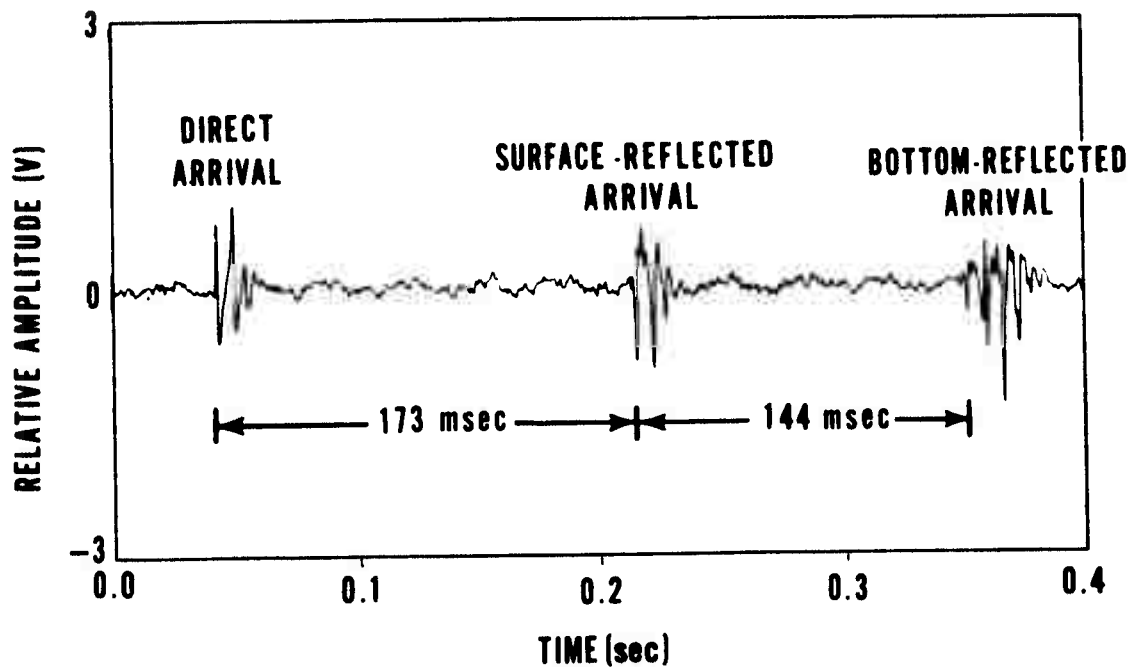
Figure 2.   Geometry of Experiment and Example of Acoustic Data
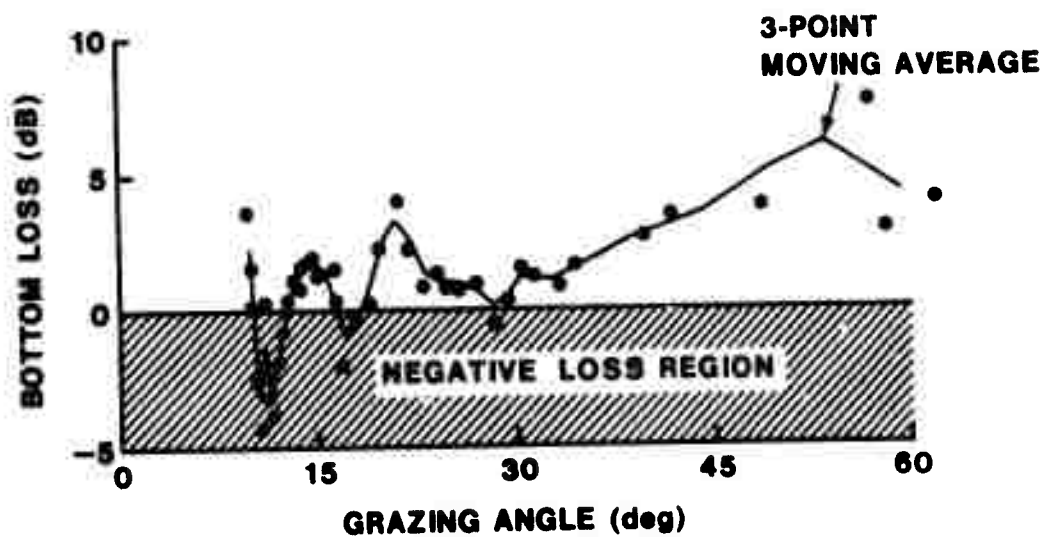
Figure 3.   Low Frequency Bottom Loss Results
(80 - 320 Hz Band)
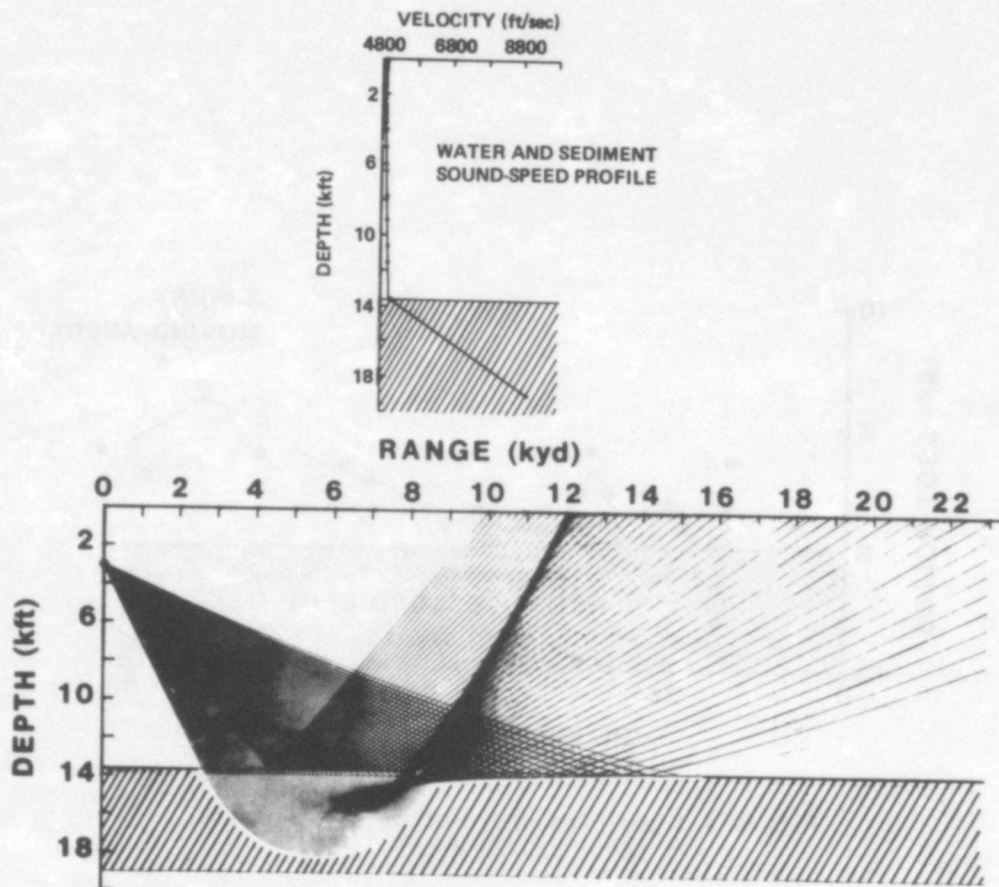
Figure 4. Ray Diagram Showing Formation of Caustic
Due to Refraction of Sound by the Sediment

II. LATERAL WAVES AND NEGATIVE BOTTOM LOSS*

INTRODUCTION

This section is intended to serve a twofold purpose. The first is to discuss one mechanism which could be responsible for anomalous bottom loss values. The second is to provide an introduction to the last two sections in which various aspects of applying deconvolution techniques to the bottom loss extraction process are discussed. These techniques have been applied to a set of simulated data. The details of the model used to generate that simulated data will be discussed here.

DISCUSSION

Plane-Wave Model

Let us begin by reviewing the point made in section I that there is a difference between bottom-reflection loss and bottom loss. If we assume that an infinite CW plane wave impinges on some arbitrary layered structure at a single angle of incidence, it is a relatively simple matter to determine the reflected field and arrive at a value for the bottom-reflection loss. If the angle of incidence is then changed and the calculation repeated, we obtain bottom-reflection loss as a function of angle at the CW frequency assumed. Under these assumptions, it is theoretically impossible for the bottom-reflection loss ever to be negative. It is also virtually impossible to make a measurement under these assumptions.

Interpreting Bottom Loss Results

As depicted in figure 5, bottom loss is determined experimentally and there are significant differences between it and bottom-reflection loss. Normally we are not dealing with an infinite CW signal, but rather with a short pulse. The wavefronts are nonplanar and multiple angles of incidence are present. The two remaining differences involve interpretation. The received pressure versus time waveform must be examined and the position interpreted as corresponding to the path ABC, in figure 5, and only that path must be identified. Lastly, it is assumed that the correction for propagation loss can be accounted for in terms of ray theory for the path ABC.

---

*This section was authored by F. R. DiNapoli

The possibility that the differences highlighted could be the cause of anomalous bottom loss results present in our data has been thoroughly examined. It is our conclusion that the difficulty does not lie with the experimental design or with the data processing procedures, but rather with the interpretation applied to obtain bottom loss results. If more energy is present in that portion of the waveform interpreted in terms of the path ABC, then anomalous bottom loss values can occur in both the positive and negative directions due to multipath interference effects. It is further concluded that this additional energy is not due to water column paths, but rather to that path which is pictorially shown as ADEC in figure 5. That is, energy which is incident on the bottom at some angle α interacts with the subbottom either by being reflected or refracted, including the possibility of exciting lateral waves, and then returns to the receiver time-coincident with the energy associated with the path ABC.

Semi-Infinite Fluid Model

Quantitative evidence in support of this hypothesis is obtained by considering the simplest type of environmental description (figure 6) involving acoustical interaction at a single boundary. Such a description consists of two semi-infinite ideal fluids, having constant but different sound speeds and densities. A point source emitting 100 msec, 50 Hz sinusoidal pulses is situated in the lower-speed water 305 m above the higher-speed bottom.

At any given frequency, the total field can be expressed in terms of a direct wave plus an integral which represents both the lateral and reflected waves. The time-independent solution, consisting of the direct plus the bottom-interacted waves, is given by*

$$H(z,r,f) = \frac{e^{ik_1 R}}{R} + \frac{i}{2} \int_{-\infty}^{+\infty} \frac{e^{i\beta_1(z+z_0)}}{\beta_1} V(\xi) H_0^{(1)}(\xi r) \xi d\xi. \quad (5)$$

Asymptotic methods are usually invoked to solve the integral. These methods provide results which can be physically interpreted when the grazing angle is not too close to the critical angle. If the grazing angle is considerably greater than the critical angle, we obtain a single expression which can be interpreted in terms of the reflected field,

Grazing Angle >> Critical Angle

$$H(z,r,f) \simeq \Psi_{reflected}.$$

When the grazing angle is much smaller than the critical angle, the two terms in the asymptotic result can be identified with the reflected and lateral waves,

Grazing Angle << Critical Angle

$$H(z,r,f) \simeq \Psi_{reflected} + \Psi_{lateral}.$$

*Mathematical terms not defined in this synopsis can be found in reference 4.

For angles close to critical, however, uniform asymptotic methods must be used,

$$\text{Grazing Angle} \simeq \text{Critical Angle}$$

$$H(z,r,f) \simeq \Psi,$$

and unfortunately it becomes impossible to interpret the results physically in terms of only the reflected or lateral wave. It is our opinion that this is not the result of using an inappropriate mathematical formulation, but that for angles close to critical the two waves are inseparable. Now recall that a critical assumption made in the bottom loss approach is that the energy associated with only the bottom-reflected path could be identified. Our opinion is that this is a physical impossibility for angles close to the critical angle. Thus additional energy is present which cannot be accounted for by ray theory, and anomalous bottom loss values will result. In order to obtain quantitative evidence to support this claim, the exact total field was simulated using the Fast Field Program[4] and these data were then processed according to the previously discussed bottom loss extraction process.

Mathematical Process

An outline of the mathematical process is given by equations (6), (7), and (8). The time domain solution for the pressure field is obtained by multiplying the transfer function of the medium, $H(z,r,f)$, with the frequency spectrum of the input waveform, $F(f)$,

$$\tilde{p}(z,r,t) = - i2\pi\rho\int_{-\infty}^{+\infty} F(f)H(z,r,f)e^{-i2\pi ft}fdf. \tag{6}$$

The transfer function is given by

$$H(z,r,f) = \underbrace{\frac{e^{ikR}}{R}}_{\text{Direct Path}} + \underbrace{\frac{i}{2}\int_{-\infty}^{+\infty} \frac{\overbrace{V(\xi)e}^{\text{Reflection Coefficient}}}{\beta_1} \, {}^{i(z+z_0)\,\beta_1} \, \overbrace{H_0^{(1)}(\xi r)\xi d\xi}^{\text{Hankel Function}}.}_{\text{Bottom-Interaction Path}} \tag{7}$$

If the Hankel function is approximated by the first term in its asymptotic expansion,

$$H_0^{(1)}(\xi r) \approx \sqrt{\frac{2}{\pi}} \; \frac{e^{-i\pi/4}}{\sqrt{\xi r}} \; e^{i\xi r}$$

and $\xi_m = \xi_0 + m\,\Delta\xi$, $r_n = r_0 + n\Delta r$, $\Delta\xi\Delta r = 2\pi/M$, the field integral can be considered as a Fourier transform.

The transfer function can then be written as the discrete Fourier transform

$$\mathcal{H}(z, r_n, f_p) \approx \frac{e^{ikR}}{R} + A_n \sum_{m=0}^{M-1} (E_{m,p}) e^{i2\pi mn/M}. \qquad (8)$$

The impulse response, which is not shown, is obtained by taking the Fourier transform of the function. Equation (8) was evaluated at 1024 discrete frequencies and the previously described convolution procedure yielded a time history for the 100 msec, 50 Hz sinusoidal pressure waveform at many ranges.

Simulated Data

The waveform at the left of figure 7 is for a range where the grazing angle is greater than the critical angle, and thus the lateral wave has not been excited. The amplitude of the waveform agrees well with the ray theory prediction. Agreement is denoted by the lines above and below the waveforms. The middle waveform results at a range where the grazing angle is slightly less than the critical angle. The lateral wave is excited and destructively interferes with the reflected wave. Ray theory is in error, because it cannot account for the effect of the lateral wave. The waveform at the right is for a far range where the angle is considerably less than critical. Although the lateral wave is excited, there is no time-coincident contribution and agreement is found between amplitudes.

Impulse Response of Simulated Data

The impulse response for the direct path portion of the field is a delta function which is reduced in amplitude by the length of the direct path, and delayed in time by the travel time needed for the signal to get from the source to the receiver.

The impulse response for that portion of the field which has interacted with the bottom is shown in figure 8 at the same ranges used in the figure 7. At a range where the grazing angle is greater than the critical angle, shown at the left, a time-delayed delta function is obtained, which is reduced in amplitude by the magnitude of the reflection coefficient in addition to the path length. The next impulse response corresponds to a range where the grazing angle is slightly less than critical, and both the reflected and lateral waves are time-coincident at the receiver. The similarity between this result and that shown to the left is evident, and at this range it is physically impossible to interpret the impulse response in terms of solely a reflected or lateral wave component. The impulse response to the right corresponds to the range where the lateral wave could be time-separated from the reflected arrival. The lateral wave portion of the impulse response starts with the positive steplike excursion. At this angle, the reflection coefficient has a magnitude of one and a phase which is very close to 180°. This enables us to associate the reflected portion of the impulse response with the large negative spike.

Determining Bottom Loss from Simulated Data

Simulated waveforms for a considerable coverage in range were processed in a manner analogous to the relative bottom loss measurement approach. These results are compared in figure 9 with those obtained from the theoretical bottom-reflection loss formulation. As expected, for higher grazing angles, where the lateral wave has not been excited, the bottom loss curve agrees well with the bottom-reflection loss curve obtained by using the Rayleigh reflection coefficient. Good agreement is also found at small grazing angles, because although the lateral wave is present, it arrives time-separated from the bottom-reflected wave. Between roughly 10 and 35 degrees, the bottom loss curve differs significantly from the Rayleigh curve. This is also expected, because they differ precisely over the angular region in which the reflected and lateral wave signals are coincident in time. Anomalous values occur in both the negative and positive directions.
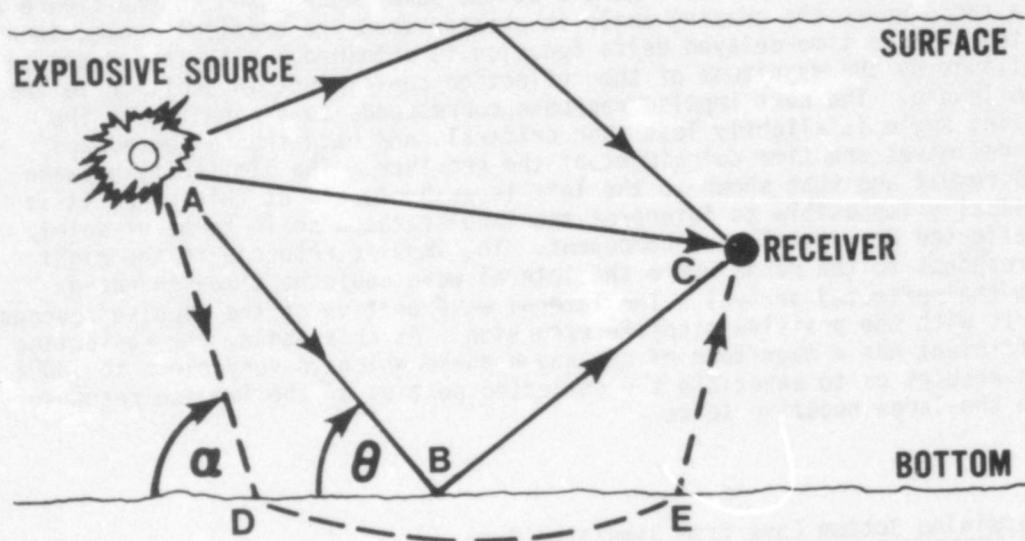
Figure 5.   Acoustic Paths That Must Be Considered When
Interpreting Relative Bottom Loss Measurements Results
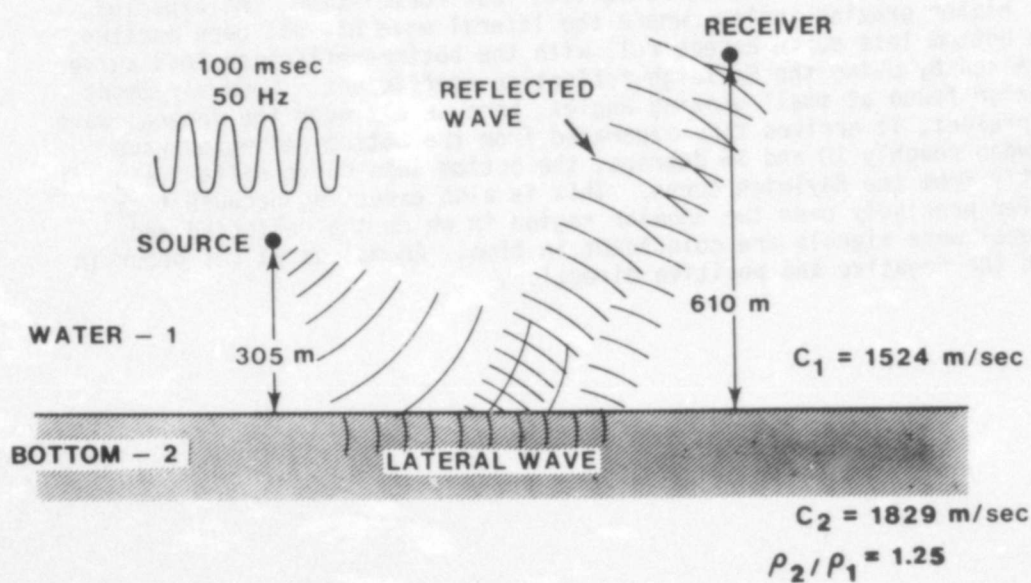
Figure 6.   MODEL: Two Semi-Infinite Fluids When
Reflected and Lateral Wave Interactions at
Boundary (Bottom) Is Considered
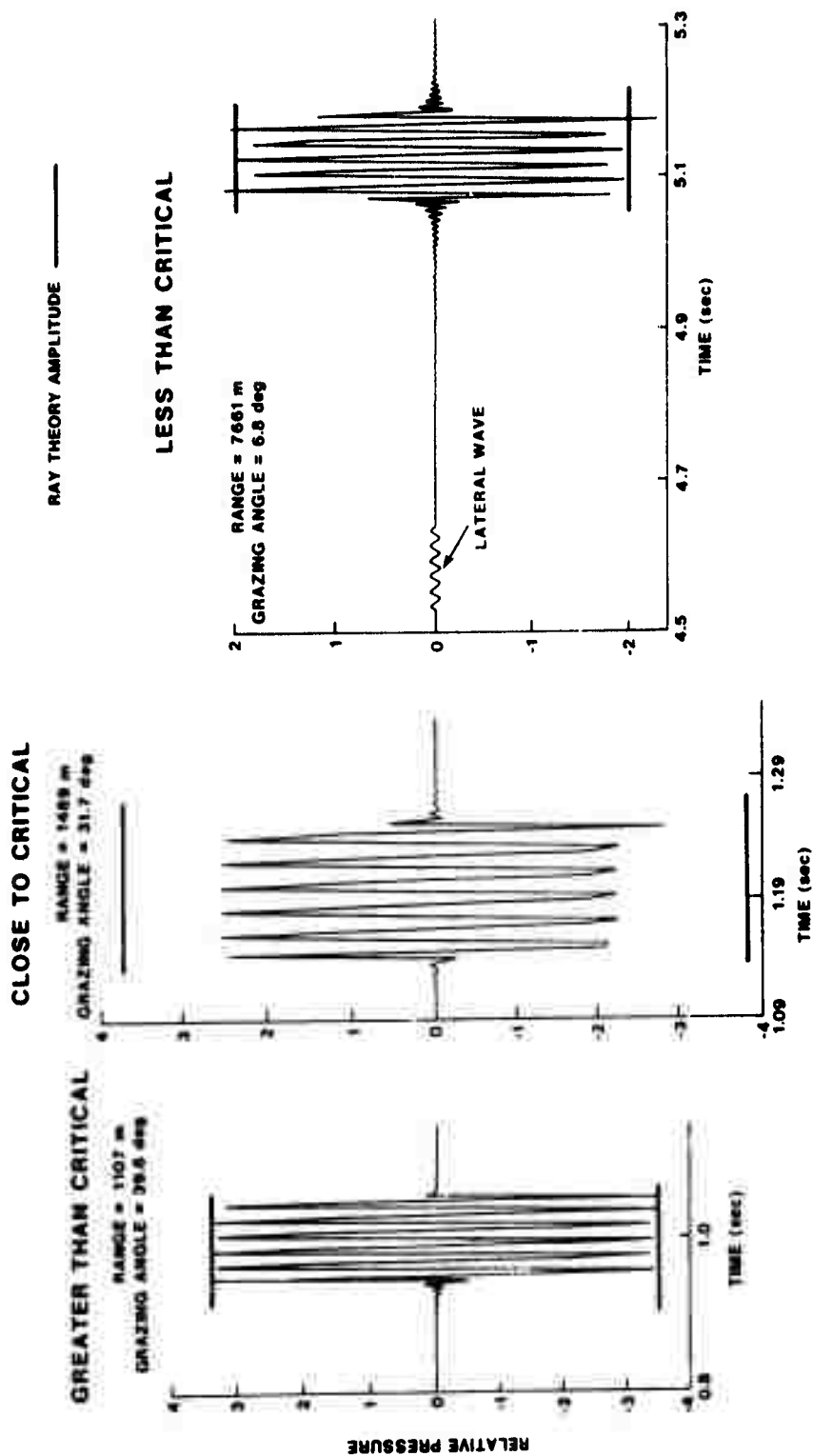
Figure 7. Modeled Waveforms for Various Ranges and Grazing Angles
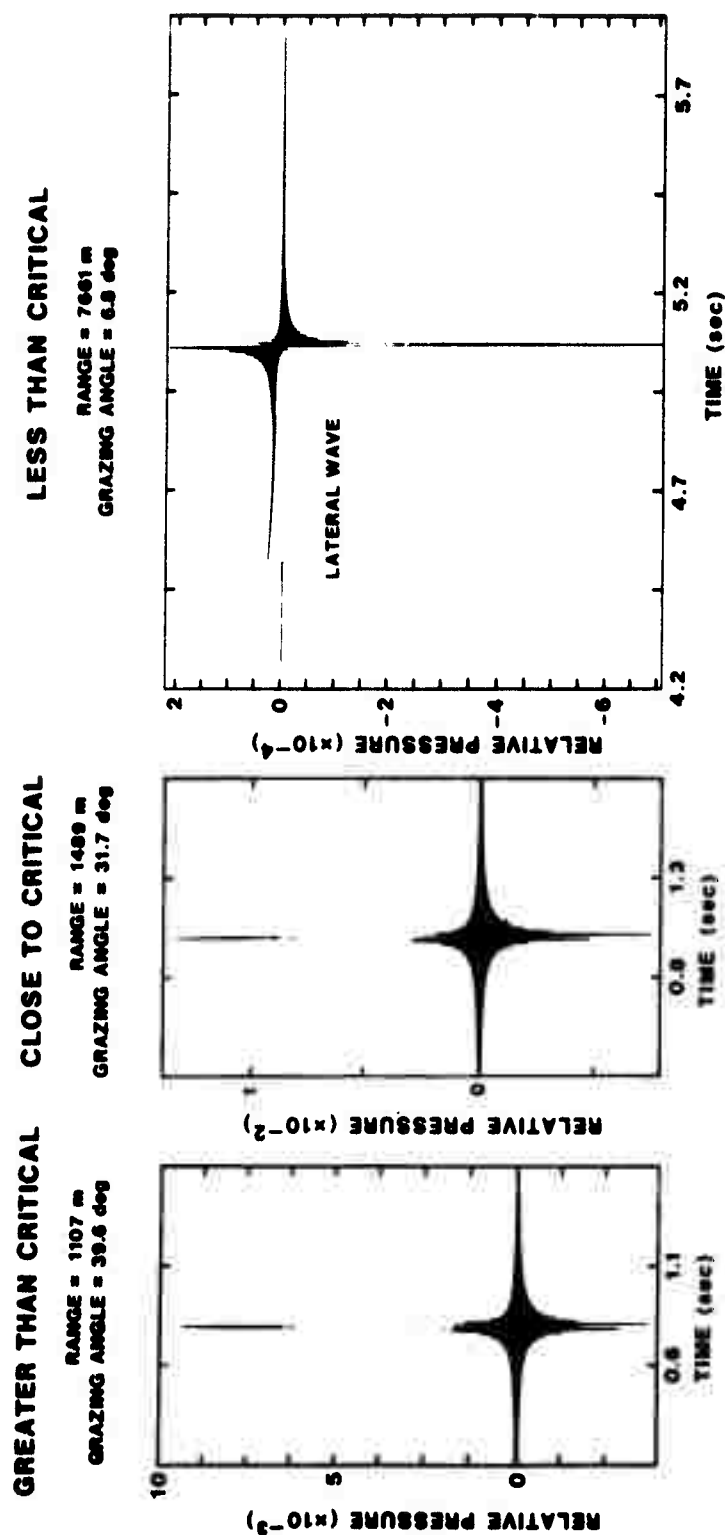
Figure 8. Modeled Impulse Responses for Various Ranges and Grazing Angles
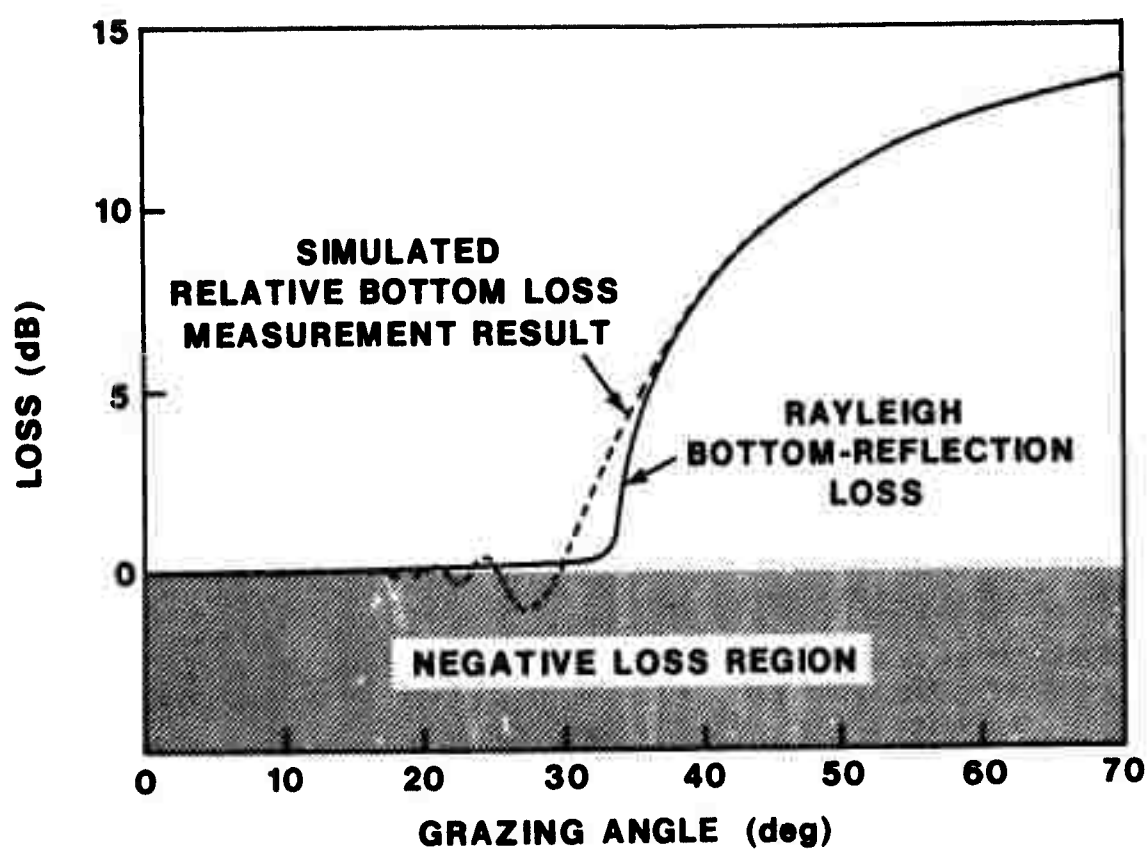
Figure 9. Rayleigh Bottom-Reflection Loss Curve and Modeled
Relative Measurement Bottom Loss Curve When Reflected
and Lateral Wave Interaction Was Considered
in Deriving Bottom Loss Curve

III. DECONVOLUTION OF LOW FREQUENCY OCEAN-SEDIMENT ACOUSTIC SIGNALS -- SIMULATION STUDY*

INTRODUCTION

Ocean bottom acoustic measurements are often conducted by using transient acoustic signals, such as explosives. The waveform resulting after transient acoustic signal interaction with the sediment can be too complex to infer sediment acoustic properties. However, if the sediment mechanism can be approximated as a linear system, deconvolution can be used to obtain the sediment acoustic impulse response. The impulse response can improve the ability to infer sediment acoustic properties. Unfortunately, deconvolution is limited by noise in incident and received signals. The previous section described a study which simulated the time record of a pulsed CW signal after propagation through a semi-infinite ocean and interaction with a semi-infinite sediment. This section summarizes the results of an additional simulation study[5] where received signals both in the absence and presence of broadband Gaussian noise are deconvolved to obtain the impulse response of the ocean/sediment medium. The limiting effect of noise on deconvolution is shown.

DISCUSSION

Sediment Interaction as Convolution

Consider an acoustic source in the ocean projecting omnidirectionally to a receiver. The upper part of figure 10 depicts the path of the received sediment interacted signal. The sediment interaction mechanism can be conceived as a linear system operating on an input $x(t)$ to produce an output $y(t)$. The output signal is the convolution of $h(t)$, the acoustic impulse response of the sediment, with $x(t)$, the incident signal. The sediment impulse response can be computed from the received signal by the deconvolution process.

One advantage of deconvolution is that effects which occur when water-region arrivals time-overlap and interfere with the sediment interacted signal can be reduced by improving time resolution. Each water-region direct acoustic path arrival is represented approximately by a single spike after deconvolution, and thus are time-separated from the sediment impulse response. The second advantage is that since the sediment impulse response is the response to a delta function, reflected and refracted mechanisms may be more easily distinguished, so sediment properties such as layer structure, velocity gradients, etc., can be more readily inferred. One disadvantage of deconvolution is that the process requires an acoustic time record of the source signal. The second disadvantage is that the impulse response is degraded by noise.

---

*This section was authored by P. D. Herstein and F. R. DiNapoli.

Obtaining Impulse Response Using the Transfer Function

The sediment acoustic impulse response,

$$h(t) = IFT(H(f)),$$ (9)

Transfer Function

is the inverse Fourier transform of the transfer function. By definition, the transfer function

$$H(f) = \frac{Y(f)}{X(f)}$$ (10)

is the quotient of the sediment interacted signal's complex spectrum $Y(f)$ divided by the source signal's complex spectrum $X(f)$. However, the function deteriorates and becomes unstable when $X(f)$ and $Y(f)$ contain noise,

$$x(t) = s_i(t) + n_i(t)$$ (11)

$$y(t) = s_0(t) + n_0(t).$$ (12)

This deterioration occurs because noise introduces error in estimates of $Y(f)$ and $X(f)$, and also because when noise is present in $X(f)$, artificial singularities can occur in the transfer function. In reality, the source signal time sequence $x(t)$ - equation (11) - and the received signal time sequence $y(t)$ - equation (12) - will always contain noise along with signal. A transfer function (equation (13)) lessening the effects of noise can be developed from equation (10).

$$H(f) = \left[\frac{Y(f) \cdot X^*(f)}{\langle |X(f)|^2 \rangle + A} \right] \cdot G(f),$$ (13)

Averaging   Stabilization   Filtering
(Additive White Noise)

First, the transfer function numerator and denominator are multiplied by the complex conjugate of the source signal spectrum. Next, the magnitude squared or "energy" spectrum resulting in the denominator is replaced by the source signal energy spectrum ensemble averaged to reduce spectrum estimation error. The constant A, the additive white noise factor, is then added to the denominator. This constant, generally less than one percent of the total source signal energy, stabilizes the transfer function by preventing denominator values near and at zero, and thereby eliminates artificial singularities in the transfer function. Finally, the new quotient is multiplied by a filtering function $G(f)$, which filters the quotient outside the frequency band of source signal spectrum high-signal-to-noise ratio values. In this simulation study, $G(f)$ is always the constant one, independent of frequency, to show more clearly the effect of broadband Gaussian noise on deconvolution.

Comparison of Unprocessed and
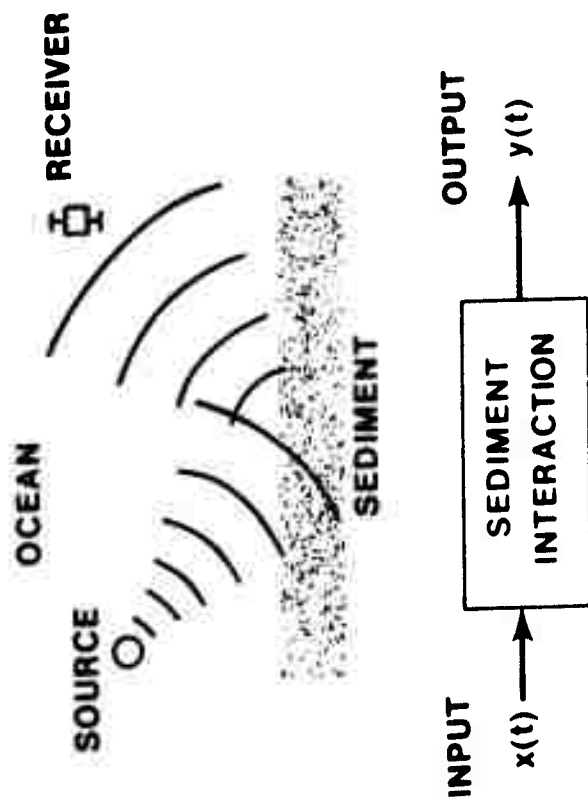## Deconvolved Signals

In this study, pulsed sinusoidal signals were simulated to propagate through the ocean-sediment model (described in section II), both in the absence and presence of broadband Gaussian noise.

In figure 11, the uppermost trace shows the unprocessed simulated received multipath signal containing both direct and sediment-interacted arrivals, in the presence of broadband Gaussian noise; the signal-to-noise ratio is approximately 18 dB. This unprocessed signal is deconvolved, using three methods. The replica source signal for all three methods is an isolated direct path arrival. The first of three deconvolved traces is computed using the unmodified transfer function; that is, the transfer function is obtained by simply dividing the received signal spectrum by the replica signal sprectrum. In this trace, neither the direct path or sediment-interacted impulse response can be distinguished from the noise. The second deconvolved trace is computed using the additive white noise factor, the constant A previously mentioned, for stabilization. The lowest trace shows the impulse response computed by using stabilization and also ensemble averaging eight replica source signal spectra to reduce variance. Here the impulse response of the direct and sediment interacted arrivals can be seen distinctly.

The effect of noise on deconvolution as a function of grazing angle was visually recorded by a computerized movie, which outlined the model geometry and methodology. The movie further showed the time-history ocean-sediment impulse responses derived by deconvolving the simulated signals, first in the absence and then in the presence of broadband Gaussian noise. In the presence of noise, stabilization and averaging were used.

The movie is available upon request to the authors of this section. Highlight frames of the film are contained in NUSC Technical Memorandum TA11-311-75.

THE ACOUSTIC IMPULSE RESPONSE OF THE SEDIMENT

SOURCE

OCEAN

RECEIVER

SEDIMENT

INPUT

OUTPUT

$x(t)$

$y(t)$

SEDIMENT
INTERACTION

SEDIMENT INTERACTION APPROXIMATED BY CONVOLUTION

$$y(t) = \int_{0}^{+\infty} h(t') x(t-t') dt'$$

Figure 10. Sediment Interaction Mechanism Approximated
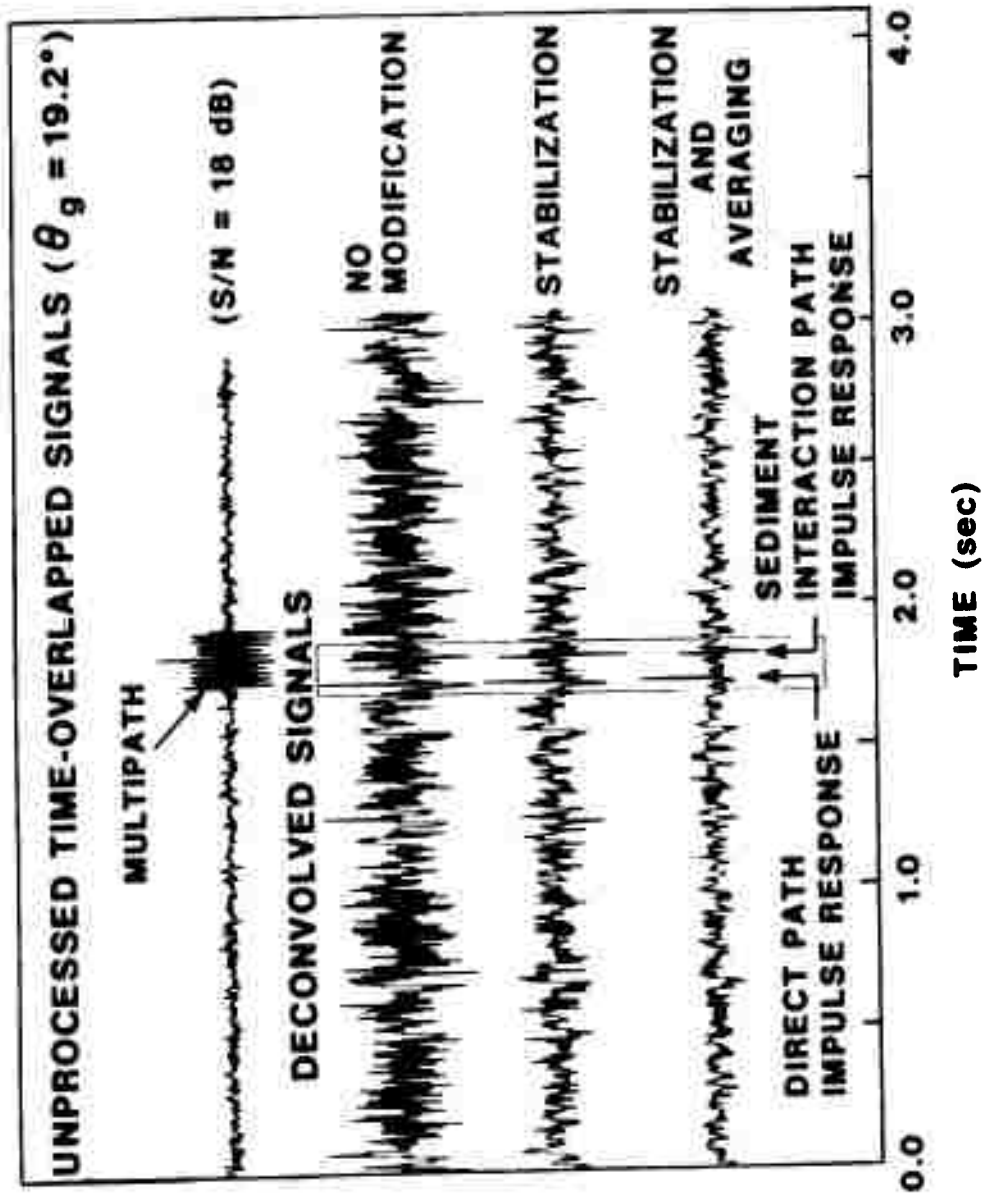As a Convolution Process

Figure 11. Unprocessed and Deconvolved Signals Showing Improvement in Deconvolved Signals With Stabilization and Averaging

IV. DECONVOLUTION OF LOW FREQUENCY OCEAN-SEDIMENT
ACOUSTIC SIGNALS -- EXPERIMENTAL MEASUREMENTS*

INTRODUCTION

As described in sections I, II, and III, ocean bottom reflectivity is a complex mechanism involving propagation phenomena such as the interaction of subbottom reflected and refracted acoustic waves. This section will concern itself with an additional complicating factor which occurs in the experimental measurement of ocean bottom loss at low frequencies and over wide bandwidths: the interference from bubble pulses generated by explosive sound sources. However, with the aid of deconvolution, bubble pulse interference effects can be eliminated, and an accurate description of subbottom multipath structure can be obtained. From an analysis of this improved description of the ocean bottom's response to acoustic signals, the complex physical processes associated with ocean bottom reflectivity may be described and explained in greater detail.

DISCUSSION

Experiment Description

The geometry associated with the experimental data presented in this section is shown in the upper half of figure 12. Explosive charges were deployed from a surface vessel at varying horizontal ranges from a fixed receiver, to provide bottom loss data over a wide range of grazing angles. In addition to the receiver shown at a depth of approximately 1500 m, data were simultaneously obtained by a second receiver at a depth of 900 m. As can be seen in the lower half of the figure, the arrivals for a typical reception are quite distinct and separable with respect to time. With the aid of a computer ray-tracing program, horizontal range and bottom grazing angle were determined from the measured time differences between the various arrivals. The ray-tracing program also provided the water-region propagation loss for each individual arrival.

Deconvolution Processing

A simplified mathematical description of the deconvolution processing is given by equation (13) of section III. This equation was applied to the experimental data with the exception that averaging of the input spectra, $X(f)$, was not performed. The impulse response is determined by obtaining

---

*This section was authored by R. K. Dullea and P. D. Herstein.

the inverse Fourier transform of the ocean bottom transfer function which, in itself, is computed by dividing the spectrum of a given bottom arrival by the spectrum of the corresponding direct arrival. To obtain an absolute value of the transfer function, this quotient must be adjusted by a factor equivalent to the difference in propagation losses associated with the two arrivals. As discussed in section III, a Gaussian filter function was utilized in the process to improve the signal-to-noise ratio; and a small fraction of white noise was added to the direct arrival spectrum to enhance the stability of the transfer function.

Effect of Deconvolution

The effect resulting from the application of deconvolution is demonstrated in figure 13. The upper trace is representative of a typical time series from an unprocessed reception. The shock wave and associated bubble pulses of the direct arrival are clearly defined. Because of bubble pulse interference in the unprocessed bottom arrival, it is possible to identify only the reflection from the ocean-bottom interface boundary. However, in the deconvolved time series shown in the lower trace, the interference from bubble pulses has been almost totally eliminated in both the direct and bottom arrivals. As such, two additional subbottom receptions are distinctly visible in the bottom arrival. With this improvement in the acoustic response from the ocean sediment, it is possible to determine the nature of these two predominant subbottom arrivals.

Consecutive Bottom Arrivals Versus Grazing Angle

The approach to identifying the mechanisms which produce the subbottom arrivals observed in the data is demonstrated in figure 14. The time histories of bottom arrivals are displayed with respect to the bottom interface reflection and consecutive receptions are "stacked" along the ordinate as a function of the water-sediment interface grazing angle. A side by side comparison of this format both before and after deconvolution shows again the improvement in definition that is obtained from this processing technique. Although the existence of subbottom arrivals is evident in the unprocessed data shown on the left in the figure, their presence is distorted by the interference from the bubble pulses (especially in the region where the grazing angles are between 15 and 25 degrees). With the elimination of this interference by means of deconvolution, the trend in the relative time displacement of the subbottom arrivals as a function of grazing angle becomes more apparent. The incorporation of Bragg's equation[6] for reflections in a layered medium has resulted in the identification of the first subbottom arrival as that belonging to a reflection from a layer at a depth of 20 m below the water-sediment interface. The abrupt appearance of the second subbottom arrival at a grazing angle of approximately 25 degrees, and its subsequent rapid convergence with the subbottom reflection for decreasing angles are characteristic of a refracted arrival from a medium having a velocity gradient. This identification was achieved with use of the Ewing and Worzel[7] equation describing refractions. In addition to the identification of the two predominant subbottom arrivals, it should be noted that the amplitude of these receptions is significantly greater than that of the interface reflected arrival for grazing angles less than 25 degrees. An

example of the effect that the interaction of these arrivals has upon the total received energy from the ocean bottom is shown in figure 15.

Comparison of Power Spectra of Direct and Bottom Arrivals

As described in section I, ocean bottom loss can be determined by measuring the relative energy level difference between time-isolated direct and bottom receptions. In the comparison of the power spectra of the direct and bottom arrivals shown in figure 15, the energy level of the bottom arrival has been increased by a value corresponding to the difference in propagation loss between the two arrivals; thus, the difference between the power spectra is equivalent to the ocean bottom loss. However, because of constructive interference between the strong subbottom reflected and refracted arrivals which compose the total bottom arrival, certain regions in the spectrum exhibit a difference indicative of a "negative" bottom loss. The comparison presented here is complicated by the interference between the shock wave and bubble pulses which result in the peaks and nulls observed in the power spectrum of the direct arrival. With the aid of deconvolution, this complication can be removed.

Ocean Bottom Transfer Function

By calculating the Fourier transform of the direct and bottom impulse responses determined by means of deconvolution, bubble pulse interference in the frequency domain is eliminated and an accurate representation of the ocean bottom power transfer function is obtained as shown in figure 16. As a result, the peaks and nulls now observed in the time-isolated, composite bottom spectrum are solely a result of the interaction between the bottom interface and subbottom arrivals. For example, the time difference between the dominant subbottom reflected and subbottom refracted arrivals associated with the event depicted in figure 16 was approximately 15 msec. This time difference corresponds to a $\lambda/2$, or π-radian phase difference, between the tow arrivals at a frequency of about 100 Hz. Thus, we would expect mutual destructive interference (or a spectral null in the transfer function) to occur at this frequency and at odd integer multiples of this frequency (namely, at about 300, 500, 700 Hz and so on, as seen in figure 16). Conversely, we would expect that below 100 Hz and also at even integer multiples of this frequency, mutual constructive interference (or spectral peaks) should occur as is displayed by this curve. The time difference between the various bottom arrivals is critical in the determination of the resultant ocean bottom transfer function; hence, it is important to investigate the possibility of variations in the transfer function at a fixed interface grazing angle as a function of experiment geometry.

Variation of Ocean Bottom Transfer Function
With Receiver Depth

Hydrophone receivers were located at depths of 900 and 1500 m during the experiment, and a comparison was made of the ocean bottom transfer function measured at these two depths with reference to a fixed interface grazing angle, as shown in figure 17. As can be seen, significant differences do occur in both the amplitude and shape of the transfer functions as a function of receiver depth. These differences are a result of variations in the subbottom multipath structure (both in time and amplitude) as seen at the two receiver locations. We conclude from this comparison that, whenever subbottom reflections and subbottom refractions are the dominant arrivals in a given composite bottom reception, ocean bottom loss as a function of interface grazing angle will also be dependent upon source/receiver depth geometry. An additional but equally important conclusion that can be derived in observing these transfer functions is that bottom loss varies as a function of processing bandwidth. For instance, if we desired the level of bottom loss at a specific frequency which should happen to be located at or near one of the spectral nulls in the transfer function, the bottom loss value that one would obtain would be greatly dependent upon the processing bandwidth.

Bandwidth Dependence of Bottom Loss
Versus Grazing Angle

By using the comparative energy processing technique discussed in section I, bottom loss versus grazing angle was obtained at a center frequency of 100 Hz for both one-third and full-octave processing bandwidths as displayed by figure 18. As shown, three-point moving average curves have been fitted to the actual data values. Although in general there is good agreement between the two curves, significant differences are also noticeable, especially in the region for grazing angles greater than 50 degrees. Note also that, between 20 and 25 degrees, the one-third octave curve does not penetrate the negative bottom loss region as decisively as the full-octave curve. In conjunction with the previous discussion of the processing bandwidth dependence exhibited by the ocean bottom transfer function, the relative differences in bottom loss in a comparison of this type would have been even greater for a processing bandwidth narrower than one-third octave.

EXPERIMENTAL GEOMETRY

SEQUENCE OF ARRIVALS
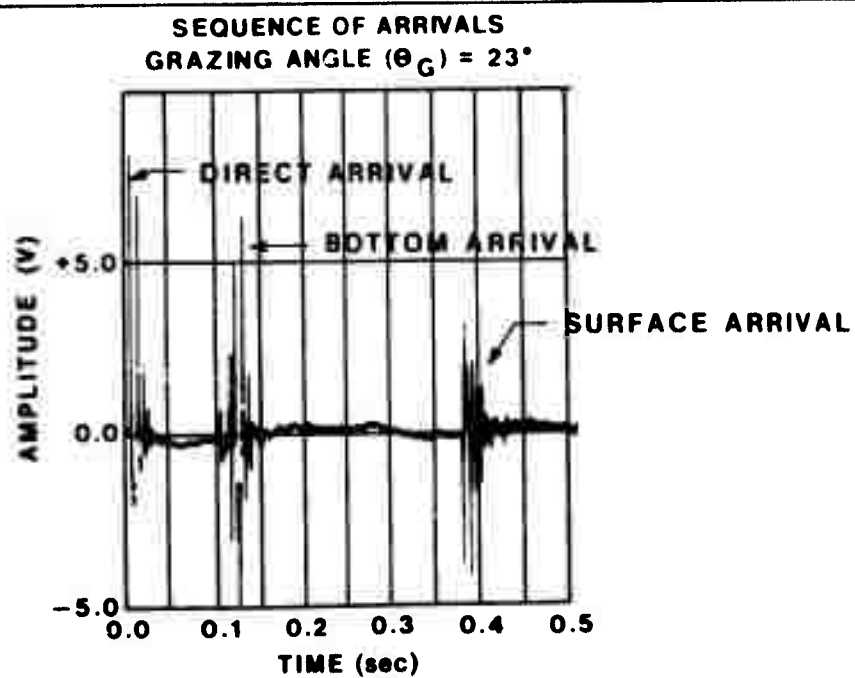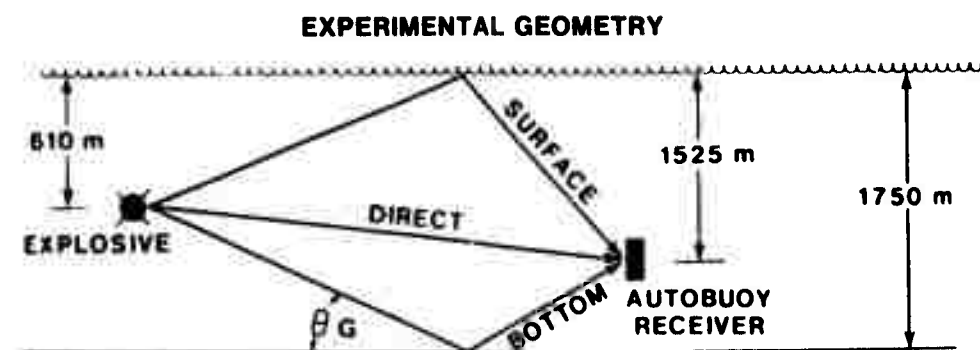**GRAZING ANGLE (Θ_G) = 23°**

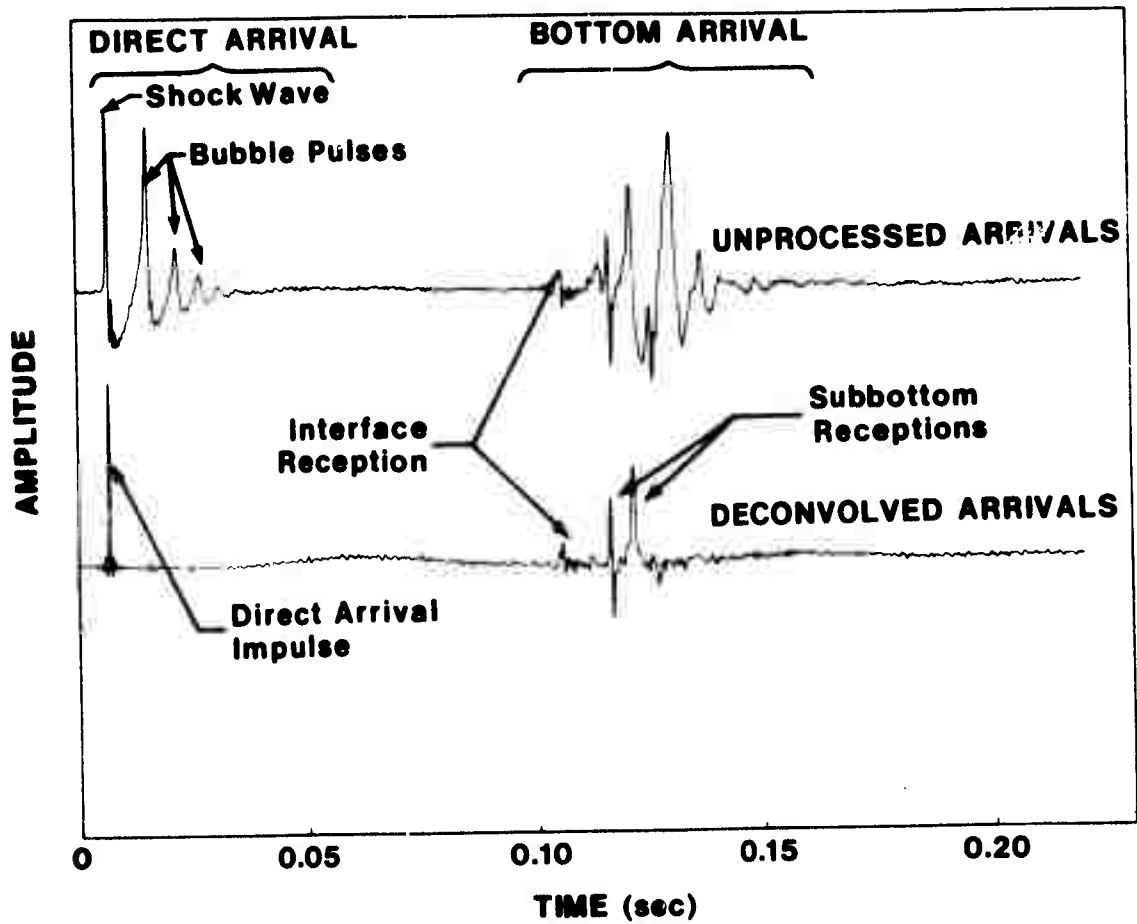Figure 12.   Geometry of Experiment and Example
of Acoustic Data

Figure 13. Signal Enhancement Derived
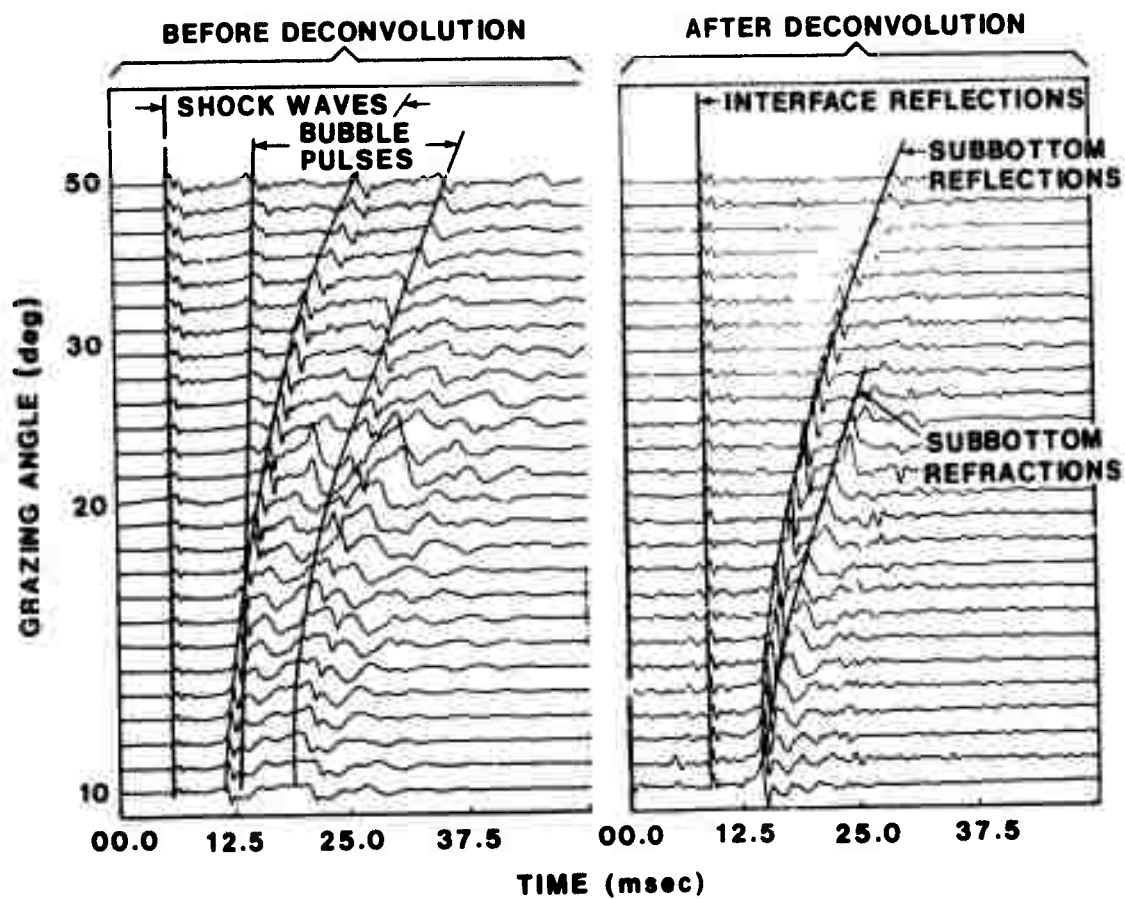from Deconvolution Processing

Figure 14. Time History of Consecutive Bottom-Interacted
Signals As a Function of Grazing Angle,
Before and After Deconvolution

Figure 15. Power Spectra of the Direct and
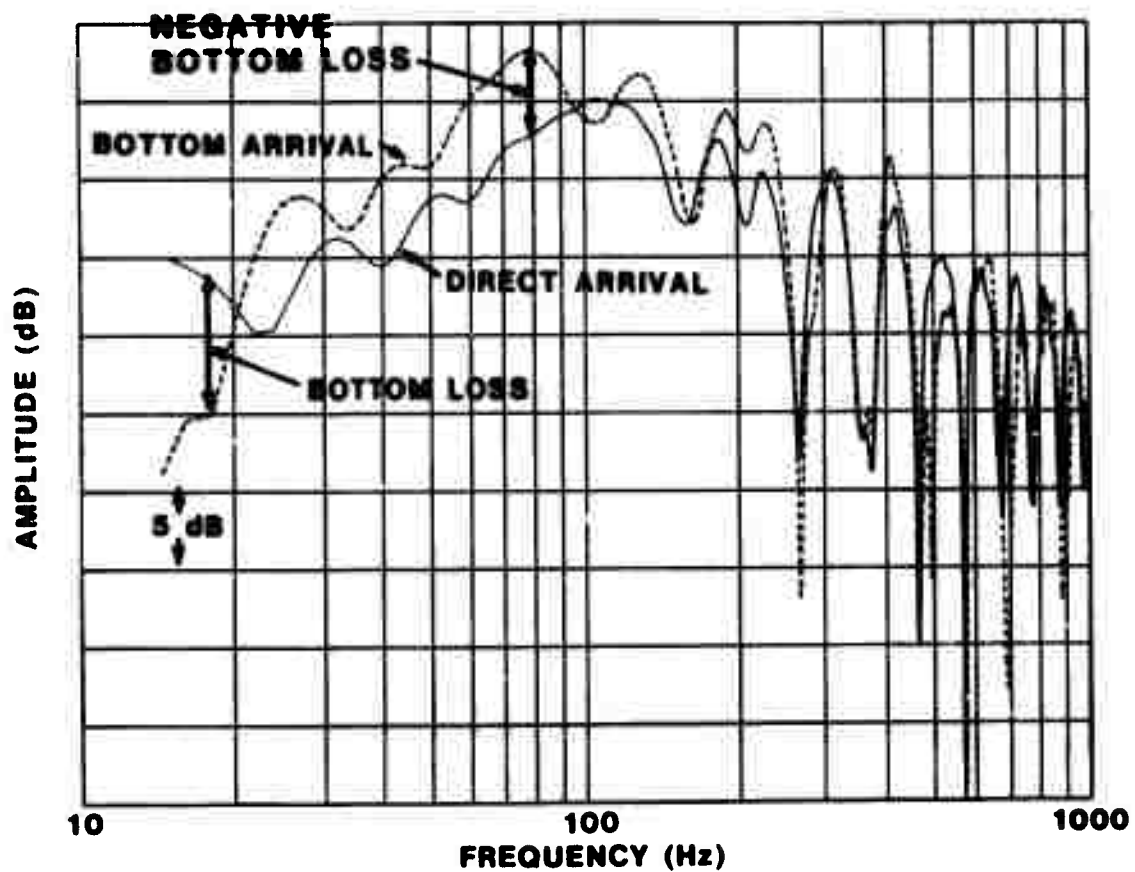Bottom-Interacted Path Signals
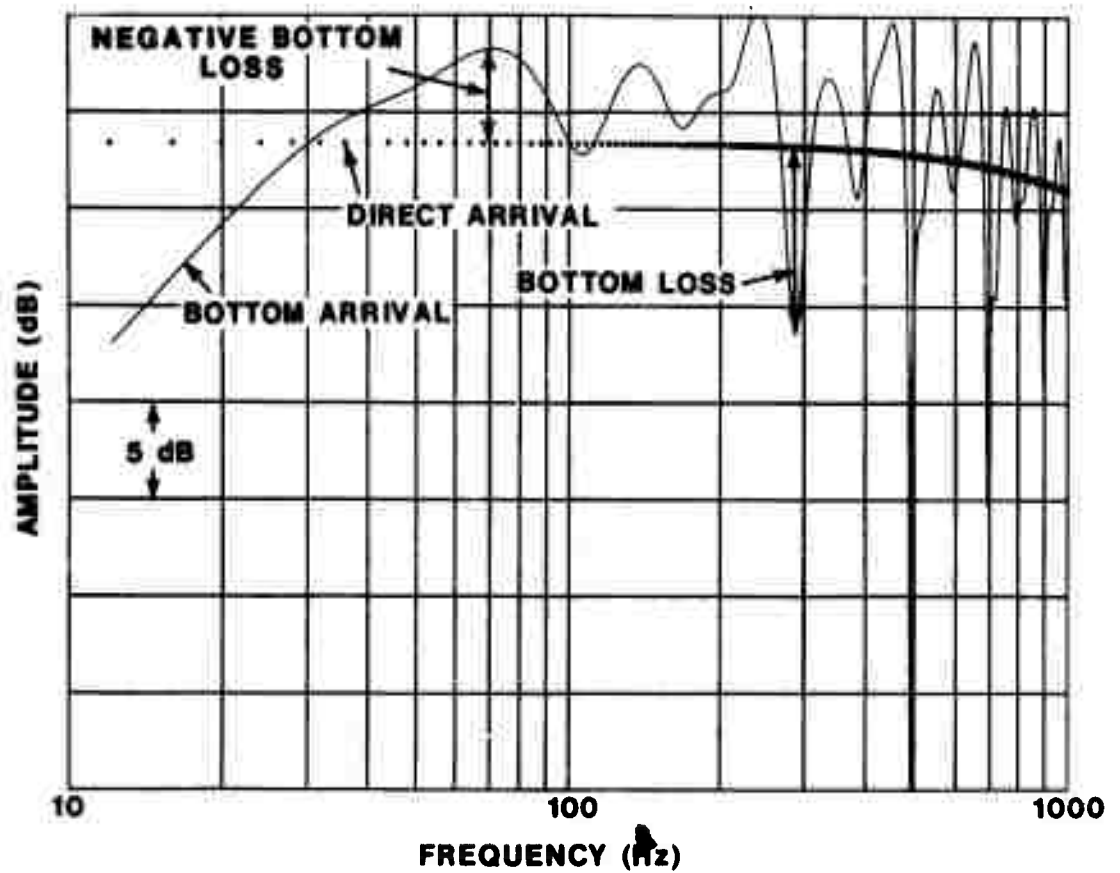(Grazing Angle = 21 deg)

Figure 16. Transfer Functions of the Direct
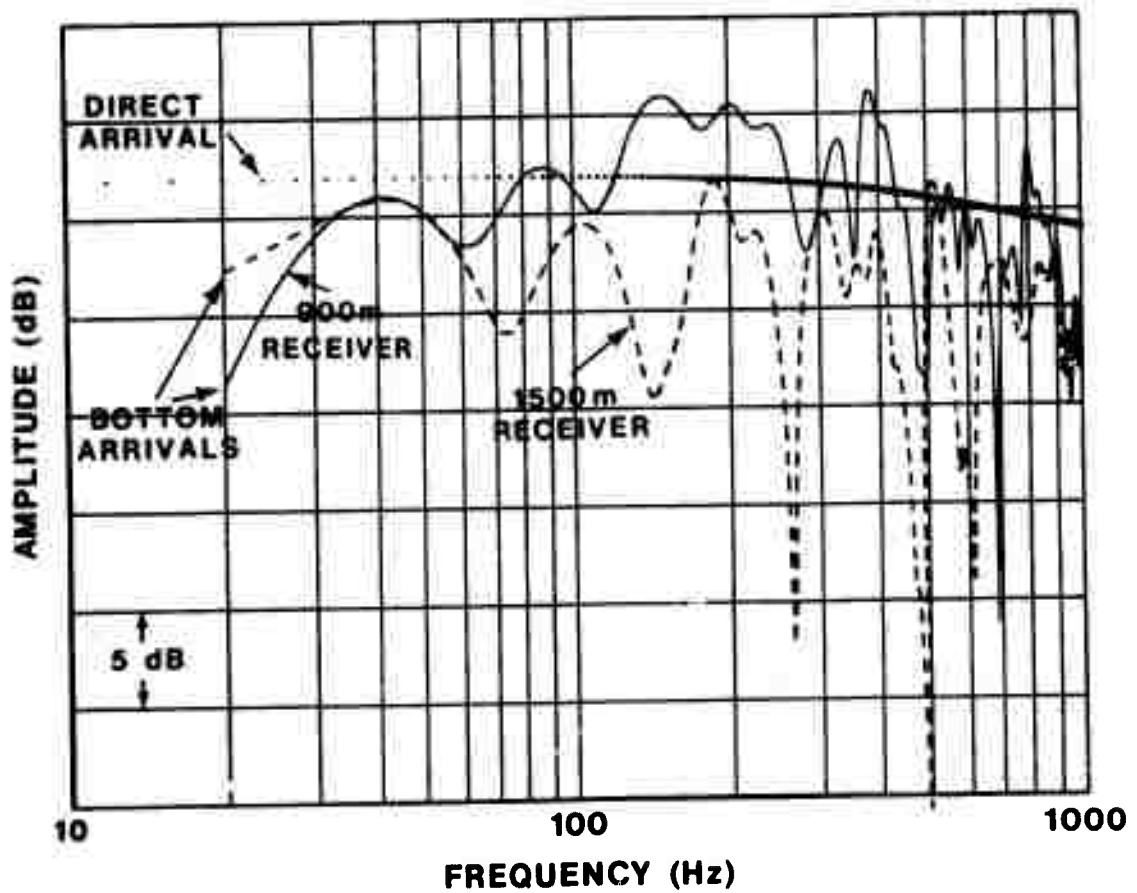and Bottom-Interacted Path Signals
(Grazing Angle = 21 deg)

Figure 17. Transfer Functions for Bottom-Interacted
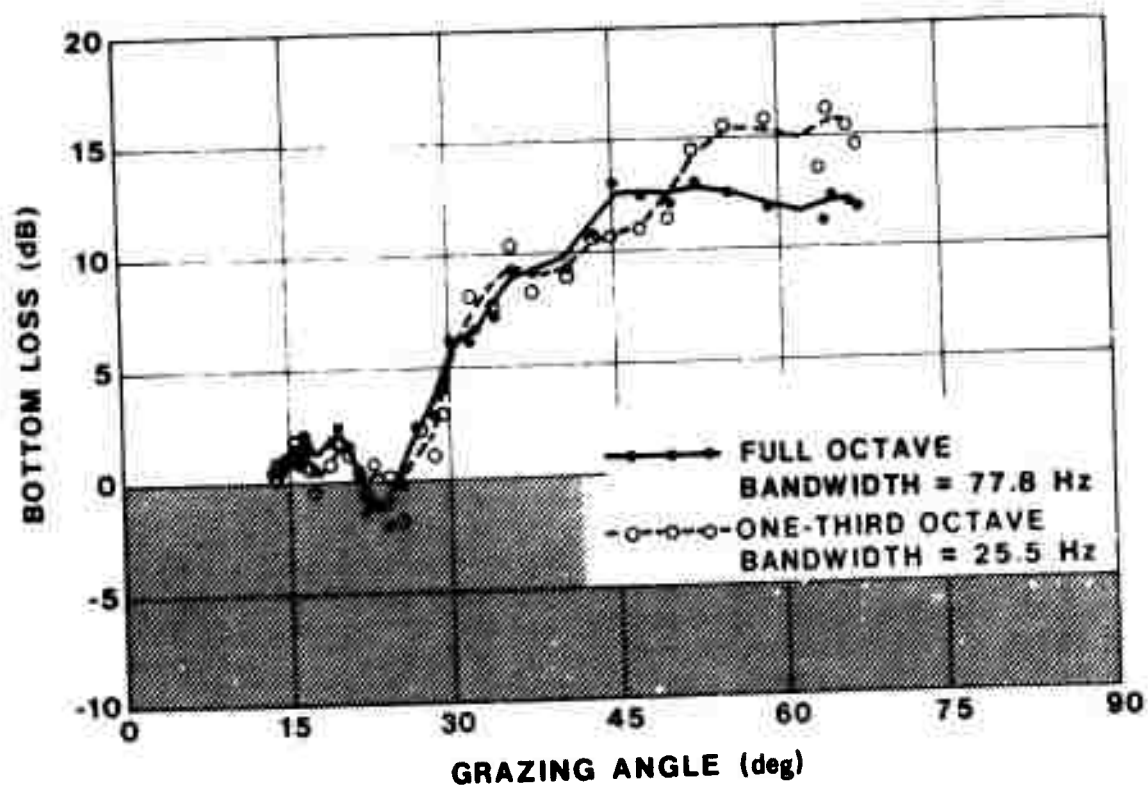Signals As a Function of Receiver Depth
(Grazing Angle = 23 deg)

Figure 18. Bottom Loss Versus Grazing Angle As a
Function of Processing Bandwidth
(Center Frequency = 110 Hz)

V. SUMMARY

Ocean bottom reflectivity is generally described by a single function: the reflection coefficient, which is defined as a ratio of reflected-to-incident intensities. The logarithm of this coefficient is called BOTTOM-REFLECTION LOSS. Measuring bottom-reflection loss within the constraints of the definition is virtually impossible. In practice, it is estimated by (1) measuring the propagation loss of pulsed acoustic signals that traversed along the path which interacted once with only the ocean bottom, (2) calculating only the water-region propagation loss for an idealized bottom-reflection path by assuming a flat, single-interface bottom having a reflection coefficient of one, and (3) comparing the values measured minus the calculated. The difference between the measured and calculated values is called BOTTOM LOSS. The above assumption inherently ignores subbottom refraction and reflection of sound, important effects at low frequencies (< 500 Hz). The ocean bottom, by reflecting and refracting sound, can partially focus acoustic energy within the water column, and if sound returning from the subbottom constructively interacts with sound returning from the water-sediment interface, the analysis can yield negative bottom loss values.

To aid in interpreting bottom-interacted pulsed-acoustic signals acquired using a relative bottom loss measurement approach, a simplified two semi-infinite fluids model, was constructed such that a CW point source and a receiver were located above the boundary and in the lower sound-speed fluid. The total field was mathematically expressed in terms of two integrals associated with the direct, bottom-reflected and sediment lateral waves (in the real ocean). These waves were simulated in the time domain using the Fast Field Program (FFP). The model-generated waveforms were processed similar to the relative bottom measurement approach and the BOTTOM LOSS curve was compared to the Rayleigh BOTTOM-REFLECTION LOSS curve acquired under the same boundary conditions. Differences occurred between these curves in both the negative and positive directions. The bottom loss curve showed negative values over precisely the angular region where the reflected and lateral wave signals are coincident in time; the Rayleigh curve, by definition, cannot show negative values. The bottom loss curve and the bottom-reflection loss curve are each correct, but in the final analysis one is not truly representative of the other. Although the model discussed herein considered the effect of only the sediment lateral wave, it provides sufficient evidence that subbottom reflected and refracted energy can interact with the reflection from the water-sediement interface, and extracted bottom loss values should not agree with the Rayleigh plane-wave model, especially at lower frequencies.

However, another difference that normally exists between measurements and predictions of bottom loss is that measurements are usually performed with wide bandwidth explosive sources, whereas predictions are made for CW signals. This requires additional processing to aid in interpreting results. Bubble pulses generated by the explosive sources complicate interpretation, but deconvolution processing can remove bubble pulse contamination and yield the impulse response of the ocean sediment. The deconvolution process is degraded by noise, and methods to reduce the noise sensitivity of the process were developed.

The FFP propagation model described above was used in a simulation study to examine the reflected and lateral wave interaction at the sediment modeled boundary. To obtain the acoustic impulse response of the simulated sediment, deconvolution was performed; i.e., the spectrum of the sediment interacting acoustic signal was divided by the spectrum of the transmitted (direct path) signal and then the inverse fast Fourier transform was computed. Controlled amounts of Gaussian noise were added to simulate ambient noise. Even low levels of noise (S/N $\cong$ 20 dB) were found to degrade the process to a point where the deconvolved signal was no longer discernible. The degree of degradation was determined by comparing reflected and lateral waveforms, after deconvolution, obtained in the absence and presence of noise. To significantly reduce the noise degradation, two processing techniques were performed: (1) a number of spectra (8) of the direct path (transmitted) signal in the presence of noise were averaged, and this averaged spectrum was used in the deconvolution process; and (2) a specified amount of white noise was injected into the deconvolution processor to stabilize the process.

The deconvolution processing was applied to ocean-sediment interacted acoustic signals acquired in a deep-water location. Bottom loss values obtained from the deconvolution process were in close agreement with values computed using the relative bottom loss measurement approach, when the direct and bottom interacted acoustic signals were well separated in time. Furthermore, the deconvolution process enchanced the clarification of the acoustic path structure within the sediment, and thereby provided experimental verification of the contention that the interaction of ocean-sediment interface-reflected arrivals with subbottom reflected and subbottom refracted arrivals can produce negative bottom loss values. It has also been demonstrated that, as a result of this type of interaction, bottom loss can be (1) experiment configuration dependent, and (2) processing-bandwidth dependent at a given frequency.

Thus the refraction of sound by the ocean sediments can have a dominant influence on the transmission process at low frequencies. To study low frequency propagation, models must accommodate the environmental description of both the water column and the ocean bottom. If such a model had been available for predicting the propagation loss of only bottom-interacting arrivals, the difference between measured and calculated propagation losses would have been a measure of model accuracy (primarily a measure of the accuracy of the environmental-acoustic description of the sediment) and not a measure of the magnitude of bottom loss.

Current efforts at NUSC are consequently oriented toward determining if seism'c reflectivity information is suitable as model input parameters for accurate low frequency propagation loss prediction. All that may be required in the future to predict low frequency propagation loss, in areas where the ocean bottom plays an important part, is ocean-sediment acoustic-parameter data (in conjunction with the water column environmental data) of the type acquired on a regular basis by many oceanographic and geological institutions involved with seismic exploration.

VI. REFERENCES

1. R. J. Urick, <u>Principles of Underwater Sound for Engineers</u>, McGraw-Hill, New York, 1967, p. 115.

2. S. R. Santaniello and P. D. Herstein, <u>Labrador Basin Low Frequency Bottom Loss Measurements</u>, NUSC Technical Report 4711, 12 March 1975.

3. R. S. Gozzo and R. L. Martin, <u>AUTOBUOY: Present Capabilities and Planned Modifications</u>, NUSC Technical Report 4505, 11 June 1973.

4. F. R. DiNapoli, <u>The Fast Field Program for Multilayered Media</u>, NUSC Technical Report 4103, 26 August 1971.

5. P. D. Herstein, <u>The Effect of Noise on the Deconvolution of Ocean Sediment Interacted Acoustic Signals</u>, NUSC Technical Report 5373, 11 June 1976.

6. D. Halliday and R. Resnick, <u>Physics for Students of Science and Engineering</u>, Wiley, New York, 1960.

7. M. Ewing and J. L. Worzel, "Propagation of Sound in the Ocean," <u>Geological Society of America</u>, Memoir 27, 1948.

INITIAL DISTRIBUTION LIST

No. of Copies

Addressee

CINCLANTFLT
CINCPACFLT
CINCEASLANT (CDR Fowke)
SACLANT C-32
COMSUBLANT (1) (R. C. Chapman) (CDR Mueller)
COMSUBPAC
COMSUBDEVGRUONE
COMSUBDEVGRUTWO (CDR Dobes, J. Seaton)
ASN(R&D) Code 102, 102-OSC(2)
ONR, Code 102-OS, 412-3, 480, 481, 786, AESD 460, 462
CNO, OP-095, -098, -098T, -96, -96C, -96C1, -981G, -981H, -955F
CNM, MAT-03, -03L, -03L4, -034-1, SP-20, ASW-14, -22, -23, -10,
    -11, 20
DDR&E (G. Cann)
NRL, 2627, 8101, 8167, 8168, 8170, 7206, 9320
OCEANAV
NAVOCEANO, Code 02, 037, 3000, 7200, 9200, 9320, 03, 06, 6130, 3600
NAVAIRSYSCOMHQ
NAVELEX, Code 320, 03, PME-124, 124T, 124TA, 124-20, 124-30,
    124-40, 124-60
NAVSEA, SEA-03, -03C, -034, -0341, -06H1, -06H1-1, -061H1-2,
    -06H1-3, -06H1-4, -06H2, -09G3, -660, -661, -660G-22(Yang)
NAVAIRDEVCEN
DTNSRDC
NAVCOASTSYSLAB
FLEET ASW TACTICAL SCHOOL (CDR Breuggeman)
NAVSURFWPNCEN
NELC
NAVUSEACEN
NAVPGSCOL (W. Cunningham, A. Leipper)
DARPA, Code TTO (CAPT Cox)
APL/UW, Seattle
ARL/PENN STATE, State College
Center for Naval Analyses (Acquisition Unit)
DDC, Alexandria
Marine Physical Lab, Scripps
ENV RES LAB NOAA/ERL
COMMITTEE UNDERSEA WARFARE
WOODS HOLE OCEANOGRAPHIC INSTITUTION (J. Ewing)
Lamont-Doherty Geological Observatory (R. E. Houtz, H. Kutshale
ARL - University of Texas